Int J Adv Manuf Technol (2017) 90:2363–2376
DOI 10.1007/s00170-016-9533-0

ORIGINAL ARTICLE

Three-dimensional modeling of the stress evolution in injection molded parts based on a known melt pressure field

Kristjan Krebelj[1] · **Nikolaj Mole**[1] · **Boris Štok**[1]

Received: 12 July 2016 / Accepted: 25 September 2016 / Published online: 15 October 2016

Abstract To obtain the initial conditions for ejection analysis of an injection molded part, a numerical simulation of the stress evolution in the material during injection molding is required. This topic, described in the literature only modestly for the full three-dimensional geometry, is addressed here by proposing an approach simple enough to be implemented in a general purpose solid mechanics simulation code. This feature makes it especially suitable with respect to the analysis of ejection, where custom code development might present hindering amount of additional work. As temperature and pressure field evolutions are obtainable through a computational fluid dynamics analysis, they are taken as input data in the stress analysis. The novelty of the approach is in the treatment of the melt region, where explicit tracking of the melt-solid interface is substituted by imposing the known pressure field in the melt region. The validity of the approach is experimentally tested by analyzing shrinkage and mass of moldings, as well as partial cavity pressure evolution at different packing pressure settings.

Keywords Injection molding · Numerical simulation · Residual stresses · Shrinkage · Ejection

✉ Nikolaj Mole
nikolaj.mole@fs.uni-lj.si

Kristjan Krebelj
kristjan.krebelj@fs.uni-lj.si

Boris Štok
boris.stok@fs.uni-lj.si

[1] Faculty of Mechanical Engineering, University of Ljubljana, Aškerčeva 6, 1000 Ljubljana, Slovenia

1 Introduction

After introducing the topic, some works on ejection analyses are examined to highlight the motivation for the work herein. Next, a review of the literature dealing with shrinkage and residual stress prediction is given and commented. Lastly, a brief relation of this work to the published research is presented.

By means of numerical simulation, individual stages of the injection molding cycle can be inspected, which aids achieving of the required final product's properties and optimization of the process parameters. In general, reducing the amount of corrective work during mold development also contributes to decreasing of the related costs and production delays. Historically, the numerical analyses were first aimed at modeling only the filling stage and were later extended to the analysis of the packing stage and product shape prediction (the history of the development of numerical modeling of the injection molding process is described by Kennedy [1]). This follows from the fact that each subsequent stage of the cycle depends on the previous stages. The last production stage—ejection—was thus addressed only after the predictions of residual stresses were available. These contributions were few and hindered by the fact that the material state of a product during an injection molding cycle was demanding to predict numerically, especially for non-simplified three-dimensional geometry. One reason was also the lack of adequate computational power at the time, which is becoming a lesser issue nowadays with the progress of computing technology, thus making way for further development in the field of modeling.

Our motivation is to provide a foundation for the ejection analyses, so they can be initiated with a closer approximation of the material state at the time of ejection. The stress

evolution modeling falls within the scope of the final product geometry and stress state prediction, which is required to analyze product performance—typically, the final product geometry is of interest.

1.1 Motivation in ejection analysis

Wang et al. [2] analyzed the effect of different ejector-pin layouts on the ejection force of a product. The filling and packing stages were simulated with the use of a custom developed code, described by Kabanemi et al. [3]. This code was limited to thin-walled product geometry. Pontes et al. [4] analyzed ejection using a solidification modeling approach, developed by Jansen and Titomanlio [5], where temperature and crystallization fields were predicted by filling and packing analyses, while the pressure evolution was known from experiments. The solidification model made use of readily available computational fluid dynamics (CFD) codes, which is convenient, but the geometry was limited to thin-walled axisymmetric tubular moldings. An ejection analysis was also performed by Bataineh and Klamecki [6], combining a readily available CFD code and a solid mechanics simulation code, but the report is very limited regarding the transfer of the material state description between the two simulation environments. This unfortunately holds also for the work of Marson et al. [7].

The ejection studies were based on the mid-plane approach, which is also referred to as the 2.5D approach, where product geometry is described as a system of surfaces with a thickness assignment—thin-walls. This is a significant limitation when analyzing ejection. Before ejection, a product may be "anchored" by a thread (or a similar feature), which can only be treated as fully three-dimensional. In addition, Titomanlio and Jansen [8] and Bushko and Stokes [9] have shown that mold-part contact conditions also affect in-mold shrinkage and the final shape of the product. In this regard, the prediction of three-dimensional material stress state evolution is of great importance for reliable ejection analysis.

1.2 Literature background

One of the founding contributions to injection molding numerical simulation was published by Baaijens [10]. The employed (thin-wall) assumptions were listed and a model was developed, employing a viscoelastic material description to calculate the residual stresses in the final product. Chang and Chiou [11] conducted similar work with a different viscoelastic constitutive model, while advancing the geometry description to a thin-walled box, as well as considering a cooling channel layout. Kabanemi et al. [3] analyzed a box-like product and additionally performed an experimental validation of the calculated residual stresses.

Jansen and Titomanlio [5], on the other hand, proceeded with application oriented simplifications. Dismissing the viscoelastic material modeling eliminated the need for the associated material characterization and also significantly simplified the model. They argued that the simplification introduced little effect on their results. The solidification model made use of the pressure, temperature, and crystallization evolutions obtainable by CFD analysis. This sequential coupling of fluid and solid modeling was later also used by Kamal et al. [12] on fully three-dimensional geometry with the addition of a viscoelastic material description. The solidification model contained only the solidified portion of the material by adjusting the melt-solid interface, as predicted by the preceding CFD analysis. This was in accordance with the assumption (already introduced by Jansen and Titomanlio [5]) that the melt does not withstand deviatoric stresses. Later work on the prediction of the three-dimensional material state was conducted by Kang et al. [13] and Li et al. [14]. Rigorous numerical analyses were performed with simultaneous treatment of fluid and solid. The complexity is, however, a drawback from the engineering point of view, where the manufacturing issues are the primary concern. Lastly, Spina et al. [15] developed a framework to transfer the material state description from a CFD model to a solidification model. The framework makes use of readily available software, which is desirable from the engineering point of view; however, the report does not discuss material addition within the solidification analysis, which means that the packing pressure cannot be sustained during solidification—this greatly restricts the applicability of the framework.

1.3 Proposed model in relation to published work

The current contribution proposes a fully three-dimensional counterpart of the sequential coupling of the fluid and solid modeling introduced by Jansen and Titomanlio [5]. Evolution of the thermo-mechanical state in the molded material is predicted and may be used to initiate a product ejection analysis. Because the proposed approach includes a description of the melt region, it is simpler to implement than the melt-solid interface tracking. This allows using readily available software like Abaqus/Standard in this work, making the approach more accessible to applied research, similar to the work of Bataineh and Klamecki [6] or Marson et al. [7]. For simplicity, viscoelastic material description is avoided, as done by Jansen and Titomanlio [5], but can be included in the same manner as in the work of Kamal et al. [12]. As argued by Jansen and Titomanlio [5], in amorphous polymers, the viscoelastic stress relaxation is significant in a temperature region above the glass transition temperature. In injection molding, the material typically cools quickly through this temperature region.

The proposed model was experimentally validated through shrinkage and mass measurements on polystyrene moldings

produced at different packing pressure levels. Experimental pressure evolutions are used as model input, following the practice of Pontes et al. [4], but the temperature field is calculated using Abaqus during solidification modeling. This way, having to perform a CFD analysis is avoided in this work, which is suitable for the model validation. In product design practice, however, running a CFD analysis is unavoidable, because a physical mold does not exist at the time of the analysis.

In Sect. 10, the basic concept is introduced and the governing equations are given. Section 15 describes the experimental case used to test the approach. Our (simplest possible) implementation of the proposed approach to model the experimental case is described in Sect. 23. The numerical and experimental shrinkage, mass, and partial cavity pressure results are compared in Sect. 24, where the predicted residual stresses are also shown.

2 Model formulation

After briefly discussing the essential problematics of the solid-fluid coupling, the current approach is derived from the approach of Jansen and Titomanlio [5], starting with their assumptions. The treatment of the melt region is then described in relation to the alternative approach of Kamal et al. [12]. The proposed concept is illustratively introduced by discussing the finite element (FE) method implementation. The governing equations are introduced afterward. The formulation of an FE model is omitted here, because the use of a readily available software package is suggested. An FE formulation is described by Kamal et al. [12].

2.1 The modeling concept

To model the material state in injection molding, the coupled solid and fluid phenomena need to be described. As reported by Li et al. [14], the simultaneous coupling of the two is rather challenging. The alternative sequential coupling is still attractive; this means performing a CFD analysis where the temperature and pressure fields (possibly also the crystallization field for semi-crystalline polymers) are calculated assuming a simplified behavior of the solid. These field evolutions are then imposed in a subsequent solidification model, where the main concern is the stress development in the solid.

Jansen and Titomanlio [5] made the following assumptions (here restated literally) for an injection molding thin-walled solidification model, where x and y are in-plane coordinates and z is directed through the wall thickness:

1. Continuity of stress and strain at the solid-melt interface
2. Shear stress components can be neglected in the solidified layer.
3. Uniform deformation of the solidified layer (i.e., the deformation in x- and y-directions does not depend on z)
4. The normal stress σ_z is independent of z.
5. No out-of-plane deformation during solidification
6. The solid polymer is elastic, while the melt is considered unable to withstand relevant tensile stresses.
7. Frozen-in normal (or flow-induced) stresses can be neglected.
8. Temperature, pressure, position of solid-melt interface crystallization shrinkage, and reaction shrinkage are known.

Their assumptions can be followed just as well in a three-dimensional finite element model to obtain a full three-dimensional result, which obviously does not result in a greater generality of the approach, because the geometry is still required to be wall-like to distinguish between the thickness and in-plane directions. The approach can then be adjusted to formulate the proposed generalization.

Figure 1 schematically depicts three layers of finite elements belonging to the solidified material. In accordance with assumption 6, an FE mesh is not assigned to the melt, which is assumed to apply a known pressure (assumption 8) on the material already solidified. To comply with assumptions 2–5, the in-plane displacements of a node column would be kinematically coupled (a measure that is redundant in a three-dimensional model). To advance the melt-solid interface with time, additional FEs can be introduced to the mesh to account for the newly solidified material (performed by Kamal et al. [12]). These elements should have an initial hydrostatic state equal to the current melt pressure at solidification in order to comply with assumptions 1 and 7.

2.2 Treatment of the melt region

As described in the previous section, Kamal et al. [12] have formulated a three-dimensional model where they—naturally—did not include the kinematic coupling of in-plane displacements (dismissing obsolete assumptions 2–5). The proposed concept of our work is essentially the same, but the modifications might allow a simpler model implementation—especially if it is desired to use readily available code. A possible difficulty in implementing the approach of Kamal et al. [12] is the formulation of the melt-solid interface, because an algorithm is required to find a time-dependent surface (the melt-solid interface) inside an FE mesh, as well as to apply the current local value of pressure to this surface.

To circumvent the need for such an algorithm, it is here proposed to mechanically include the melt region in the model. In this approach, the melt region is used to apply pressure on the solidified material, as is the case in practice, and a solidification criterion is then used to distinguish between melt and solid, forming the melt-solid interface implicitly.

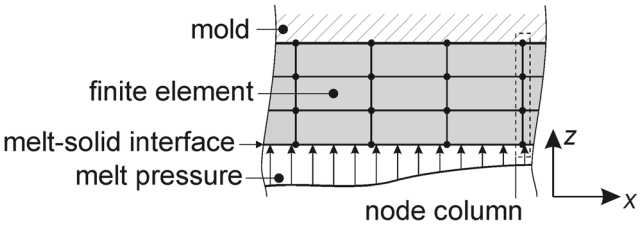

Fig. 1 An implementation of the solidification model by explicit melt-solid interface tracking

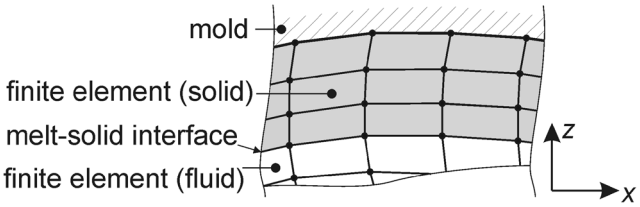

Fig. 2 Schematic representation of the proposed modeling approach

What remains is to introduce a suitable mechanical behavior of the melt region—this is performed in the following section.

2.3 Governing equations

The melt behavior in the model is determined separately for the volumetric part and deviatoric part. The deviatoric behavior is based on a modeling assumption, while the volumetric behavior incorporates the material addition, which sustains the cavity pressure. The melt region exerts a load on the solidified material, as shown in Fig. 2. The solid is assumed to follow the thermo-elastic Hooke's law.

The stress field is governed by the mechanical equilibrium equation

$$\frac{\partial \sigma_{ij}}{\partial x_j} = 0 \tag{1}$$

where σ_{ij} is the stress tensor and x_j are the spatial coordinates ($i, j = 1, 2, 3$). Tensorial notation is used, and a repeated index denotes summation over its values. The equilibrium condition (1) assumes absence of volumetrically distributed forces and inertial effects, both being negligible in the investigated circumstances. The equilibrium condition must be fulfilled for both the solid and the melt region.

A solid mechanics analysis typically begins with the whole domain already defined at the beginning, which is why it is presumed the whole cavity is already filled with the melt. This does not prevent modeling the solidification during cavity filling. To accomplish this, the temperature of the unfilled region is set to the temperature of the melt until the time of the flow-front arrival to the position, when pressure and temperature evolution are described by the CFD analysis.

In the melt region, the stress tensor σ_{ij} is decomposed into its hydrostatic component $-p\,\delta_{ij}$ and deviatoric component τ_{ij}:

$$\sigma_{ij} = -p\delta_{ij} + \tau_{ij} \tag{2}$$

where δ_{ij} is the Kronecker delta tensor and p the known melt pressure. The deformation tensor ϵ_{ij} depends on the constitutive model describing the melt. The melt volumetric deformation ϵ_{kk} can be uniquely related to the known melt pressure and temperature by the use of an equation of state, while the melt *deviatoric* deformation is of little interest when predicting the dominating thermal residual stresses in the solid because of the short fluid "deviatoric memory"; Kamal et al. [12] have therefore excluded the whole melt region from the solidification model. In reality, the deviatoric melt deformation develops large strains, hardly tractable by the Lagrangian kinematics description. Therefore, the viscous deviatoric behavior

$$\dot{\epsilon}^{d}_{ij} = \frac{\tau_{ij}}{2\,\eta} \tag{3}$$

although more realistic, is still to be avoided. In Eq. (3), η denotes viscosity and $\dot{\epsilon}^{\mathrm{d}}_{ij}$ is the deviatoric component of the rate of deformation tensor (definition is available in textbooks such as Zheng et al. [16]). The deviatoric deformation is thus proposed to be incorporated according to an elastic constitutive model

$$\dot{\epsilon}^{d}_{ij} = \frac{\tau_{ij}}{2\,Gm(p)} \tag{4}$$

where $\epsilon^{\mathrm{d}}_{ij}$ is the deviatoric component of the deformation tensor, and $G_{\mathrm{m}}(p)$ is the melt region shear modulus, which is here chosen to depend on pressure p. Equation (4) is a modeling utility, and the melt region shear modulus should be understood in the same sense; it is a parameter used to introduce deviatoric rigidity in the melt region, which prevents excessive Lagrangian mesh deformation. The introduced shear modulus should not be understood as an actual melt property. A suggestion for its value is made later in this work and the results are validated by experiments.

It remains to define the melt volumetric deformation behavior. For polymers, an equation of state is usually given in the form of specific volume $v(p, T)$. It depends on pressure p and temperature T, which are both known, while the unknown quantity is the amount of the added material maintaining the melt pressure (during filling and packing). This is described by a scalar field f, here referred to as the *mass factor* field. The field multiplies the initial mass distribution to represent the material addition. The volumetric constitutive behavior is then described by the equation

$$J = \frac{v(p, T)}{v(p_0, T_0)} f \tag{5}$$

where p_0 and T_0 are the initial values of pressure and temperature at a material point, and J is the volume ratio defined as $J = \frac{dV}{dV_0}$, where dV is the infinitesimal volume of a material point, with an initial value of dV_0. Equation (5) describes the actual volume as—obviously—proportional to the amount of contained mass. The mass factor field f is the unknown to be solved for, in conjunction to the volume ratio J. Both are initially equal to 1.

The solidified material is assumed to behave as a thermo-elastic solid according to Hooke's law

$$\epsilon_{ij} = \frac{\sigma_{kk}}{3K(p,T)}\delta_{ij} + \frac{\sigma_{ij}^{d}}{2G(p,T)} + \epsilon_{\mathrm{T}}(T)\delta_{ij} \tag{6}$$

where ϵ_{ij} denotes the strain tensor, $K(p,T)$ is the bulk modulus, $G(p,T)$ is the solid shear modulus, σ_{ij}^{d} is the deviatoric component of the stress tensor, and $\epsilon_{\mathrm{T}}(T)$ is the thermal deformation dependent on temperature T. At solidification, the strain reads $\epsilon_{ij} = -\frac{p_{\mathrm{s}}}{K(p,T)}\delta_{ij}$, complying with a hydrostatic stress state $\sigma_{ij} = -p_{\mathrm{s}}\,\delta_{ij}$, where p_{s} is the local melt pressure at solidification.

2.4 Modeling procedure and boundary conditions

The modeling procedure is summarized in Fig. 3. The initial step includes a prescription of the material properties (see Sect. 0 for the governing equations). The geometry definition is typically accomplished by the finite element discretization of the domain considered in the analysis. In case the mold is assumed rigid, only the mold cavity representing the part domain is discretized, while the rigid mold surface is considered as the fixed model boundary. In case the mold deformability is accounted for, the mold domain has to be discretized by finite elements as well (with mold material property assignment required). The initial temperature of the part domain is proposed to be the injection temperature of the melt with a zero stress tensor. The temperature and pressure field evolutions are also obtained before performing the stress evolution calculation. It is generally suggested to perform a CFD analysis with the same geometry to obtain these quantities.

The governing equations from Sect. 0 are then solved, with the temperature and pressure field evolutions imposed. The mechanical boundary condition is imposed by frictional mechanical contact at the part-mold interface. By cooling, the material inside the mold solidifies and a solid product with a non-homogeneous temperature field is obtained.

At this stage, either an ejection analysis may be performed by modeling the ejector pin loading of the part or, alternatively, the ejection may be assumed to be trivial and the ejection analysis omitted.

Finally, ejector pins and mold contact are substituted with a support which does not constrain part deformation, i.e., only the rigid body motion is prevented. The temperature is set to room temperature (or operating temperature), and the finished product geometry is determined along with the residual stresses (this also allows the determination of the product mass).

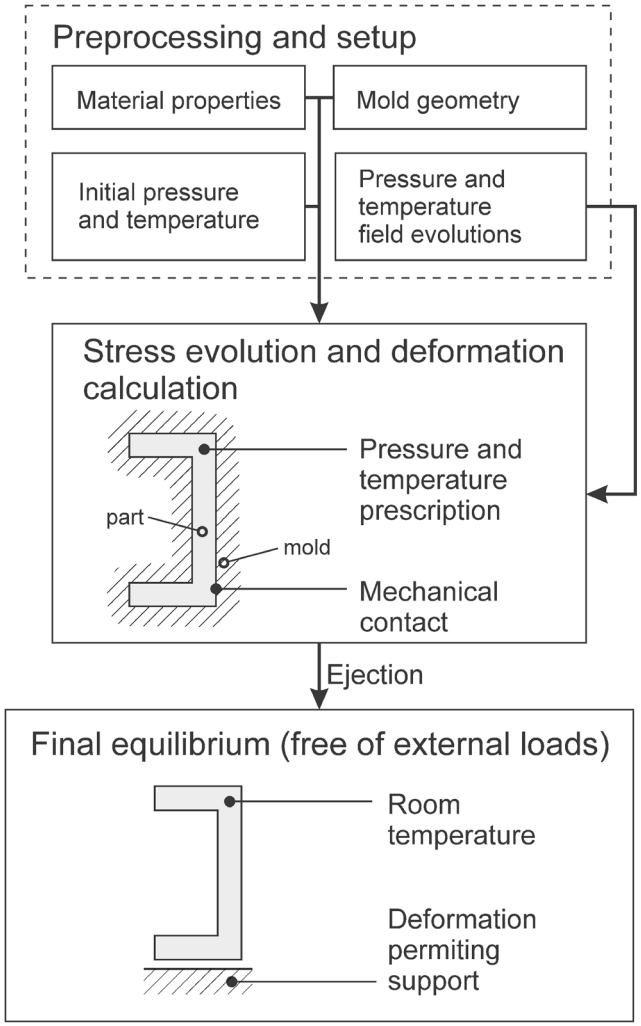

Fig. 3 Modeling procedure and boundary conditions

3 Experimental investigation

To test the proposed modeling approach, injection molding of simple plaques was performed. This section consists of a report on the measured quantities, the equipment, material choice, and experimental conditions. The measured cavity evolutions are interpreted, and details on the length and mass measurement are given.

3.1 Measured quantities

Length shrinkage is considered to be the primary quantity of interest, as it is the typical concern in product design. The validity of the final mass factor field was evaluated by

measuring the specimen mass. During the injection molding cycle, the cavity pressure, which is required as the model input, was measured, but the model relies on it only until full solidification. Afterward, the model cavity pressure is not imposed and is also compared to the measured evolution for validity. As the packing pressure was found to be the most important process parameter in regard to shrinkage by Jansen et al. [17], it was chosen to be the independent experimental variable and set to 8 different settings.

3.2 Equipment

Specimens were produced on a Boy 50M injection molding machine with a clamping force of 500 kN. The mold (Fig. 4) is an adaptation of a commercial mold for producing plaques with two symmetrically positioned cavities, of which one was considered in the investigation. Four measuring pins were installed in the mold. Three of the pins with a diameter of 8 mm were installed in the cavity under observation (Fig. 5). The measuring positions of these pins are referred to as P1, P2, and P3, successively in the filling direction. An additional pin with a diameter of 4.2 mm was used to detect the pressure in the sprue, its measuring position being referred to as P0. The height of the cavity is 1.21 mm but has an edge with a height of 1.55 mm with an in-plane width of 2.10 mm. This feature encloses the whole plaque and prevents the in-plane shrinkage inside the mold. The length, width, and height measurements of the mold cavity, displayed in Fig. 5, were computationally transformed for the operating temperature of 52 °C, while the mold geometry measurement was performed at 16 °C on a coordinate measuring machine. In obtaining the values corresponding to 52 °C, linear thermal deformation was accounted for, using the typical value of $0.12 \times 10^{-4}/°C$ for the linear thermal coefficient of steel.

Pressure applied by the melt on the measuring pins was measured using a Z1342/10000 force sensor and a Z134 amplifier, both distributed by Hasco GmbH. The amplifier output was a 0 to 10 V voltage signal sampled at 100 Hz with a 14-bit resolution, implying a discretization step of 1.22 mV in voltage and consequently 0.03 MPa in pressure measurement. A calibration procedure was performed by controlled force loading of the cavity measuring pins, according to which an error of ±1 % was estimated.

3.3 Material and experimental conditions

The material used was polystyrene (PS) Styron 678E which is a common choice in the literature, used by Jansen et al., Vietri et al., and Zoetelief et al. [18–20]. The melt temperature was set to 230 °C. The mold cooling agent (water) temperature was set to 50 °C, while the mold surface temperature during operation was measured to be between 51 and 52 °C. The filling time was approximately 0.3 s corresponding to a filling rate of about 10 cm^3/s. The packing pressure was maintained for 5 s, which was followed by additional 4.5 s of cooling. The packing pressure level was varied using eight settings in the range of 10 to 65 MPa.

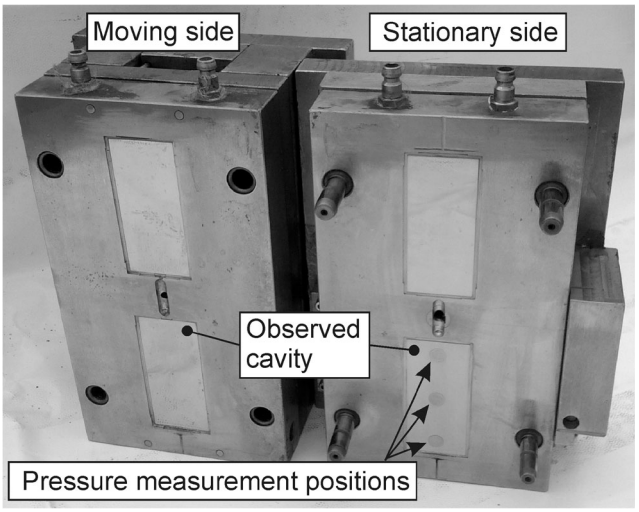

Fig. 4 Experimental mold

3.4 Cavity pressure evolution interpretation

The cavity pressure evolution is reported in Fig. 6 for the eight chosen machine settings, denoted by numbers 1 to 8. In the case of the lower four packing pressure settings (settings 1–4), the initial value of the P0 pressure significantly exceeded the value exerted during packing. The machine packing pressure release, indicated by a sharp decrease in P0 pressure, did not significantly affect the P1 pressure evolution; therefore, gate freeze-off preceded the packing pressure release and no significant back-flow occurred. For each packing pressure setting, an approximately stationary value of P0 pressure

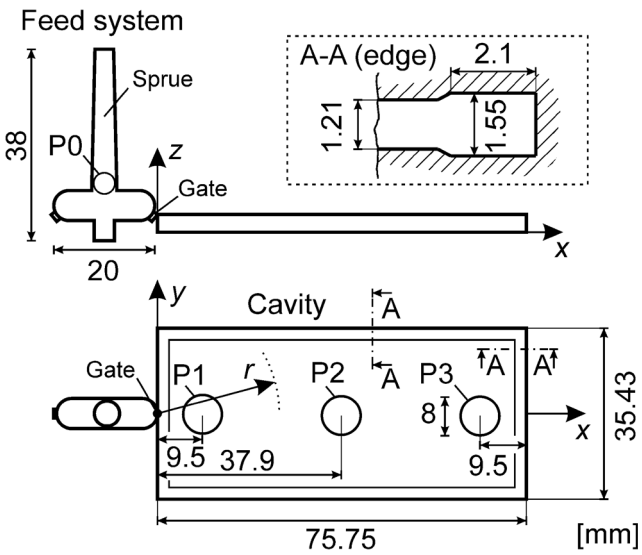

Fig. 5 Feed system and cavity

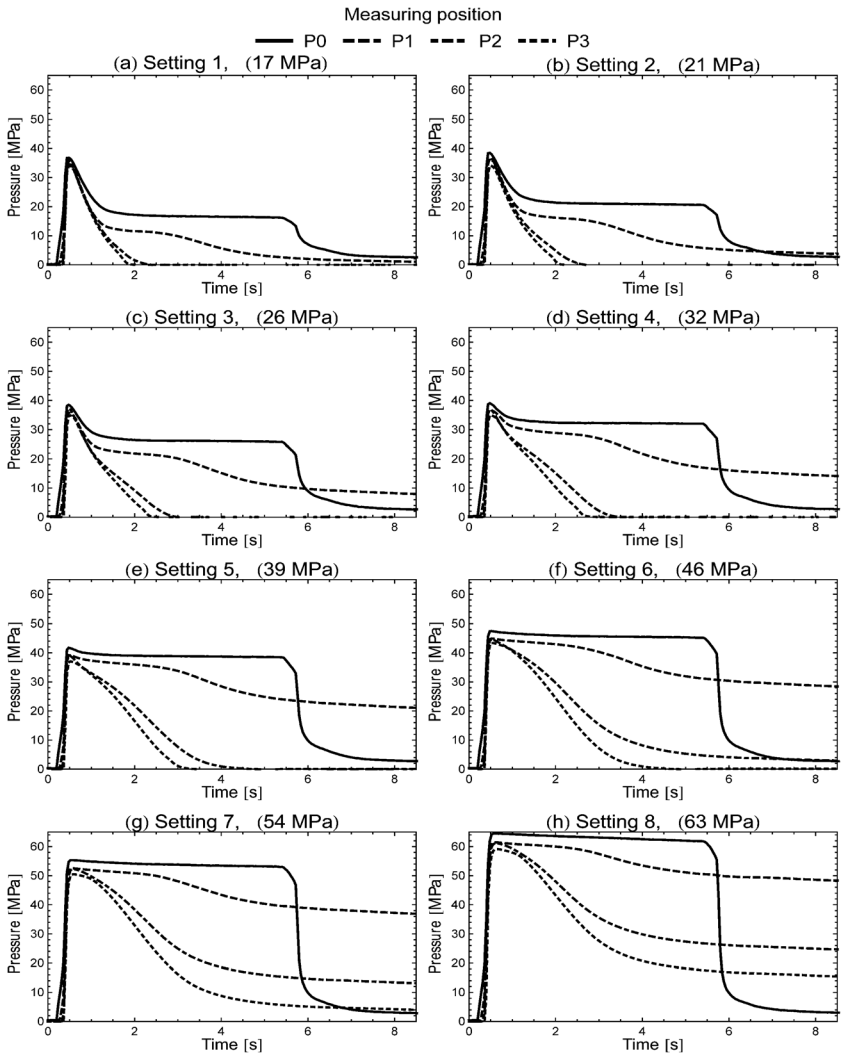

Fig. 6 Measured cavity pressure evolutions at different packing pressure settings

developed, which is given in Fig. 6 in parentheses. This value is taken as the abscissa value of respective packing pressure setting in displaying the mass and shrinkage results (see Figs. 12 and 13, respectively).

3.5 length and mass measurements

For each of the 8 packing pressure settings, 10 specimens were collected and stored at 17 °C for 24 h. Before measuring their length, they were brought to a temperature between 21 and 22 °C. Length (along the *x*-direction—Fig. 5) was measured with a "micrometer" screw gauge with a resolution of 0.01 mm, which had been installed in a positioning device, ensuring measurement repeatability. The results are later compared with the numerical modeling results (Fig. 13) as average values, measured on groups of 10 specimens. Standard deviation of the shrinkage result on all sample groups is below 0.013 %.

Mass of the specimens was measured with a Mettler B5 balance with a resolution of 0.1 mg. Average specimen mass corresponding to individual packing pressure settings was determined by measuring the mass of a group of 10 specimens and dividing the value by 10; thus, standard deviation is not available for these results. However, for one sample group, produced at a particular packing pressure setting, mass measurements were performed on each plaque individually and standard deviation of product mass of the order of 1 mg was found (at a product mass of about 3.3 g).

4 Numerical implementation of the model

To model the experimental case, the governing equations from Sect. 13 were solved by the use of a readily available FE simulation package Abaqus/Standard. The concretizations are discussed, while the particularities regarding the simulation package are largely omitted.

4.1 Indirect pressure prescription

Generally, the material pressure cannot be *directly* prescribed in a general purpose simulation code, as is the case in Abaqus.

It was, however, constrained to the known value, here referred to as the *goal value of pressure*. To achieve the indirect pressure prescription, the melt behavior—obviously—must comply with Eq. (5), and the mass factor is then continuously updated according to Eq. (5) as

$$f = J\frac{v(p_0, T_0)}{v\left(p_g, T\right)} \tag{7}$$

where the goal value of pressure p_g is taken instead of the pressure in the model p. The model pressure then converges to the goal value of pressure, and the mass factor field evolution is determined.

The mass factor field was not modified below 130 °C to account for the reduced flowing ability with cooling [21]. Also, no reduction of mass factor was applied, due to the absence of back-flow in the experiments.

4.2 Melt volumetric behavior

The volumetric behavior for polymers is usually given in the form of the Tait equation of state (see Zheng et al. [16])

$$v(T,p) = v_0(T)\left(1 - C\ln\left(1 + \frac{p}{B(T)}\right)\right) + v_t(T,p) \tag{8}$$

with the following functional relationships with respect to the transition, i.e., solidification temperature T_{tr} valid

$$v_0(T) = \begin{cases} b_{1m} + b_{2m}(T - b_5), & T > T_{tr} \\ b_{1s} + b_{2s}(T - b_5), & T \le T_{tr} \end{cases},$$

$$B(T) = \begin{cases} b_{3m}\exp(-b_{4m}(T - b_5)), & T > T_{tr} \\ b_{3s}\exp(-b_{4s}(T - b_5)), & T \le T_{tr} \end{cases},$$

$$v_t(T,p) = \begin{cases} 0, & T > T_{tr} \\ b_7\exp(b_8(T - b_5) - b_9 p), & T \le T_{tr} \end{cases},$$

$$T_{tr} = b_5 + b_6 p \tag{9}$$

The value $C = 0.0894$ in Eq. (8) is considered to be universal, while the subscripts "m" and "s" in Eq. (9) associate respective parameters to the "melt" and "solid" state, respectively. The parameters' values used in this work (material: PS Styron 678E) are listed in Table 1 as provided by Jansen et al. [18].

Equation (8), while usually not implemented in a solid mechanics simulation package, allows determining the bulk modulus K (inverse of material compressibility) by the use of the equation.

$$K(T,p) = \left(-\frac{1}{v}\frac{\partial v}{\partial p}\right)^{-1} \tag{10}$$

The volumetric thermal expansion coefficient can be obtained by the definition.

$$\beta(T,p) = \frac{1}{v}\frac{\partial v}{\partial T} \tag{11}$$

To comply with Eq. (5), the volumetric deformation needs to be additionally described in terms of the mass factor. A volumetric expansion coefficient for the mass factor is determined according to the equation.

$$k_f = \frac{1}{J}\frac{\partial J}{\partial f} = \frac{1}{f} \tag{12}$$

4.3 Melt deviatoric behavior

A value was chosen for the shear modulus introduced by Eq. (4). Excessively large deformations in the melt region are to be avoided in order to retain the FE mesh quality, but at the same time, the melt region should be allowed to change shape realistically. Specifically, significant rigidity in the melt region would couple the length and thickness shrinkage of a wall detaching from the mold surface, if its core was still molten. As a guideline for a suitable choice of the shear modulus, the following equation is proposed:

$$G_m = \frac{\sigma_M}{\gamma_M\sqrt{3}} \tag{13}$$

where σ_M is the maximal von Mises stress appearing in the melt region, and γ_M is the engineering shear strain upper limit; the σ_M can be found by first performing a simulation with a large G_m. Equation (13) is based on von Mises stress for pure shear stress state and Hooke's law for shear (see Eq. (4)). The von Mises stress in our examples did not exceed 3 MPa and with a choice of $\gamma_M = 3\%$, a melt region shear modulus was set to $G_m = 50$ MPa. This value was further reduced at vanishing pressures, when the von Mises stress in the melt area also decreases.

4.4 Mechanical behavior of the solid region

The Tait equation of state defines the bulk modulus and the thermal expansion coefficient (also for the solid)—Eqs. (10) and (11) can be used. Zoetelief et al. [20] reported the shear modulus of PS Styron 678E to be 906 MPa. This completes the definition of the elastic material behavior (Eq. (6)). Solidification was set to onset on cooling below 100 °C (as chosen by Jansen et al. [17]).

4.5 Geometry

In the numerical model, the assembly, consisting of the upper and lower part of the mold and a plaque, is formed, as shown

Table 1 Tait equation parameters [18]

	Melt	Solid	Unit
b_1	9.76×10^{-4}	9.76×10^{-4}	m^3/kg
b_2	5.8×10^{-7}	2.3×10^{-7}	$m^3/(kgK)$
b_3	1.67×10^{8}	2.6×10^{8}	Pa
b_4	3.6×10^{-3}	3.0×10^{-3}	K^{-1}
b_5	373		K
b_6	5.1×10^{-7}		K/Pa
b_7	0		m^3/kg
b_8	0		K^{-1}
b_9	0		Pa^{-1}

schematically in Fig. 7. A rectangular cuboid geometry (75.75 × 35.43 × 1.21 mm) was assumed for the plaque. In the model, the restraining effect of the edge feature which prevents in-mold shrinkage (see Fig. 5) was taken into account by constraining the in-plane displacement of the four lateral plaque surfaces (S_1 surfaces in Fig. 7). With this boundary condition, no further *mechanical* contact modeling is required on S_1 surfaces (the *thermal* contact is described later).

The deformable mold was introduced by modeling two (steel) rectangular blocks of thickness $h_M = 50$ mm, each fixed at its external surface (S_2 surfaces in Fig. 7). Poisson's ratio of 0.3 and the Young modulus of $E_M = 200$ GPa were assigned to the mold material. Considering the chosen mold thickness, the cavity deformability in the model assumes the approximate value

$$k_M = \frac{2h_M}{E_M} = 0.5\ \mu m/MPa \tag{14}$$

which is in the range of typical values according to Vietri et al. [19] and Pantani et al. [22]. Equation (14) describes the cavity deformability in the FE model based on Hooke's law. To assess the effect of mold deformability, all simulations were also run assuming a rigid mold.

The coefficient of Coulomb friction between the plaque and the mold surface was taken to be 0.4, which is an estimation based on reviewing the work of Pouzada et al. [23], who measured the coefficient of friction under ejection conditions (no empirical information for the packing conditions was found in the literature). The finite element (FE) mesh of the plaque contained 8 FEs through the plaque thickness and 160 and 74 FEs along the *x*- and *y*-directions, respectively, yielding sound FE edge size ratios of 3:3:1. The number of FEs composing the plaque was 95,000 with 109,000 nodes. The elastic mold was meshed with additional 2600 cube-shaped FEs with an edge size of 5 mm contributing further 3400 nodes to the model.

4.6 Experimental pressure evolution

The experimental pressure evolution, measured at the three cavity positions, was used to prescribe the pressure field evolution in the whole plaque domain. Note that this was possible due to the elementary geometry of the mold to aid the validation of the model. In general, however, the use of a CFD analysis is proposed to obtain the pressure field evolution.

The pressure field is obtained by assuming that the melt pressure depends only on the distance from the gate and the time. The pressure values along the radial direction *r* (see Fig. 5) from the gate were determined by a linear interpolation and extrapolation (Fig. 8) based on the pressure evolutions $p_{P1}(t)$, $p_{P2}(t)$, and $p_{P3}(t)$ at the three measuring positions P1, P2, and P3, known from the experiments (Fig. 6). For a node at a distance *r* from the gate, the pressure evolution $p(r,t)$ was thus determined. This was performed for all nodes of the plaque and prescribed as the *goal value* of the pressure field evolution. In this manner, a plausible pressure distribution is obtained, as demonstrated in Fig. 9.

To reduce the amount of the model definition data, the goal pressure evolution was prescribed as a piecewise linear

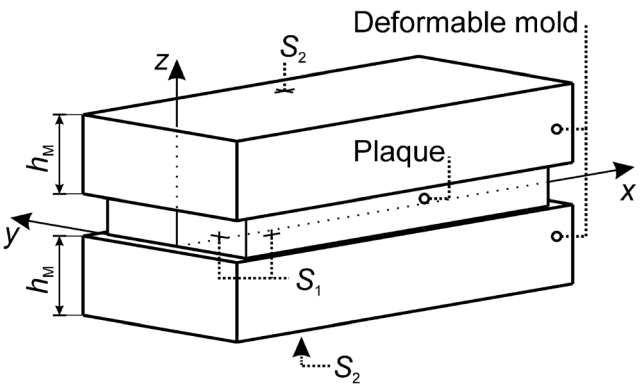

Fig. 7 Model geometry displayed schematically

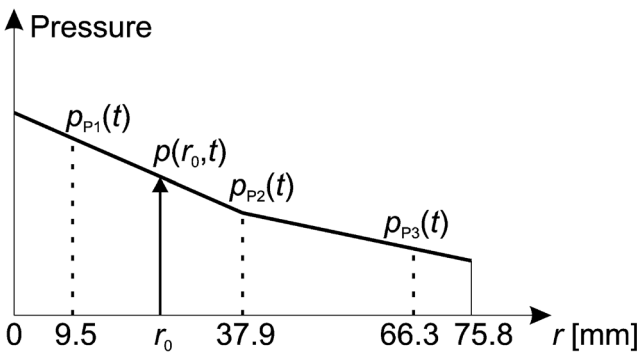

Fig. 8 Assumed distribution of the pressure along the radial direction from the gate

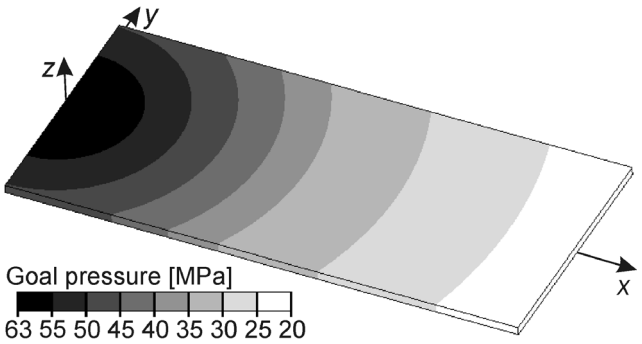

Fig. 9 Approximated goal pressure distribution at time $t = 3$ s at packing pressure setting 8

interpolation considering the respective pressure values at 40 time points ordered in a geometric progression between 0.01 and 8 s, which proved to be a sufficient approximation of the goal pressure evolution. The initial material state in the numerical model (at $t = 0$ s) is $p = 0$ MPa (at temperature 230 °C) which implies the initial plaque mass of 3.09 g.

4.7 Thermal solution

When this solidification model is applied in practice, the temperature field and the pressure field are both known from a preceding CFD analysis, because pressure measurements are not available when the mold is being designed. In this work, however, the pressure evolution was taken from the experiments, while the thermal solution was obtained by solving the heat transfer problem. The energy equation (see Zheng et al. [16]) was solved in the following form

$$\rho c_p T - \beta T p = k \frac{\partial^2 T}{\partial x_i \partial x_i} \tag{15}$$

where ρ is the mass density as defined by the Tait equation (Eq. (8)), c_p is the specific heat capacity at constant pressure, T is the absolute temperature, β is the volumetric expansion coefficient (Eq. (5)), and k is the thermal conductivity coefficient according to Fourier's thermal conduction law. The left-hand side of the equation describes the internal energy change, while the right-hand side consists of the dominant heat diffusion. Other right-hand side terms would be the viscous heating, which is neglected, and crystallization latent heat, which does not apply, because the polymer is amorphous. The specific heat for PS Styron 678E was reported by Jansen et al. [18] as shown in Fig. 10. The thermal conductivity for polystyrene was reported by Dawson et al. [24] and is given in Fig. 11.

The initial temperature of the melt was set to 230 °C, while the mold temperature of 51 °C was set as the sink temperature of the interface heat transfer condition at the plaque surface. The heat transfer coefficient in the thermal contact between the whole plaque surface and the mold was set to 1.25 kW/(m^{2}K), which is consistent with the experimental results published by Yu et al. [25], who report an evolution between 0.83 and 2.0 kW/(m^{2}K), and those of Delaunay et al. [26], who report an evolution between 1 and 5 kW/(m^{2}K). The melt completely solidified in 6 s in the mold. The plaque was then ejected and cooled down to 22 °C.

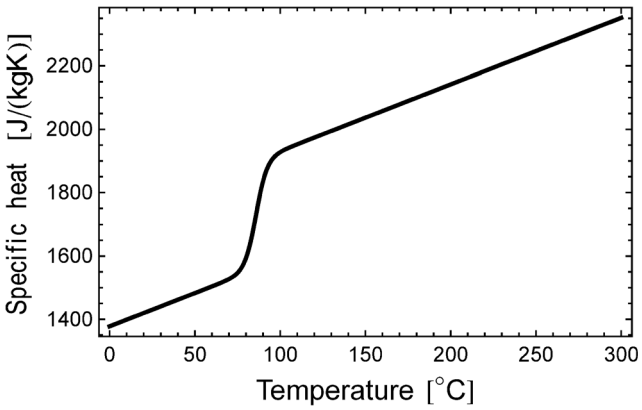

Fig. 10 Specific heat [18]

5 Results and discussion

First, the mass and shrinkage results are shown, which were obtained both experimentally and numerically. The pressure evolution in the *solidified* plaque can also be compared to the measurements. To interpret the numerical results further, the temperature evolution, the mass factor, and the residual stress distributions are also displayed. Finally, a contour plot of the transverse local shrinkage is displayed on the final geometry (with visually intensified displacements). Measured and computed shrinkage and mass results are also given numerically in Table 2 for all eight packing pressure settings.

The predicted plaque mass falls within the range of experimental values (Fig. 12) and shows a progressive characteristic

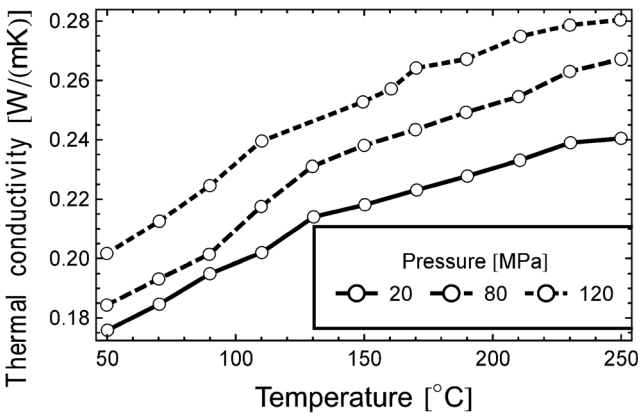

Fig. 11 Thermal conductivity of polystyrene [24]

Table 2 Measured packing pressures, shrinkage, and mass results from simulations and experiments

		Shrinkage (%)			Mass (g)		
Setting	Packing pressure [MPa]	Rigid mold	Deformable mold	Experiment	Rigid mold	Deformable mold	Experiment
1	17	0.603	0.604	0.603	3.293	3.296	3.257
2	21	0.595	0.595	0.593	3.302	3.308	3.269
3	26	0.579	0.576	0.570	3.310	3.318	3.284
4	32	0.556	0.541	0.532	3.319	3.331	3.300
5	39	0.520	0.491	0.484	3.327	3.347	3.318
6	46	0.463	0.417	0.427	3.338	3.366	3.341
7	54	0.379	0.316	0.346	3.350	3.388	3.369
8	63	0.261	0.202	0.245	3.363	3.413	3.407

with packing pressure increase. As it can be seen in Fig. 12, taking the mold deformability in consideration introduced a significant improvement in the slope prediction, i.e., the predicted sensitivity of the product mass on the packing pressure. Most importantly, the predicted mass is realistic.

The shrinkage results, as determined experimentally and numerically, are displayed in Fig. 13. The packing pressure on abscissa is taken as the time-average value of the pressure measured on position P0, during the time when an approximately constant value was maintained. The shrinkage values span a range between 0.2 and 0.6 %, which is similar as in comparable studies [17, 18]. The mold deformability affected shrinkage at higher pressures to a greater extent than at lower pressures, because the mold surface deflection increases with pressure. According to the measurements, the accuracy of the numerical prediction would suit the purpose of mold design.

The decrease in shrinkage, caused by the modeling of mold deflection, can be attributed to a difference in the cavity pressure decay, which was studied by Vietri et al. [19]. Due to mold deformability, the in-cavity pressure tends to decrease at a reduced rate, implying a higher pressure at solidification in the core and a lesser tendency towards shrinkage. Figure 14 reports a comparison between the measured pressure and the absolute value of the computed (compressive) σ_z stress in the cavity center (position P2 at mid-thickness), as determined by both of the model variations with respect to mold deformability at the highest packing pressure (setting 8). As long as the temperature is above 100 °C, the material is molten and the stress state is nearly hydrostatic. Normal stress $|\sigma_z|$ thus practically equals pressure, which from the beginning closely follows the goal value. At approximately 2.4 s (see Fig. 15), the temperature of the core decreases below 130 °C; the mass addition is ceased and the two curves representing the numerical stress evolution diverge. The case assuming the rigid mold exhibits a steeper decrease in the stress, while the case assuming the deformable mold decreases at a similar rate as measured, which confirms the adequacy of the assumed value of mold deformability k_M. The phenomenon was already demonstrated by Baaijens [10].

The temperature evolutions in the plaque center and at its surface, obtained by computer simulation of the case with the highest packing pressure (setting 8) and deformable mold considered, are depicted in Fig. 15. The solidification of the plaque center occurred at approximately 3.5 s with the decrease of temperature below 100 °C. This confirms that, according to the numerical model, the duration of 6 s of the packing and cooling in the mold is sufficient to not affect the shrinkage solution, because the plaque is allowed to solidify completely before ejection. The increase in temperature of the plaque center (for approx. 6 °C at 0.2 s) occurs due to pressurization—it is governed by the pressure term of the energy equation (see Eq. (15)).

Depending on the packing pressure setting in the simulation, the initial plaque mass 3.09 g increased during the packing phase by between 7 and 11 %. Figure 16 displays the final mass factor distribution on a longitudinal cross section of the plaque produced at the packing pressure setting 8. The final value of the mass factor increased with gate proximity,

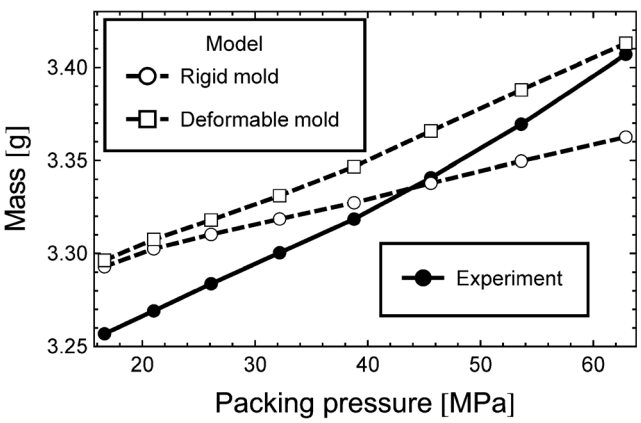

Fig. 12 Dependence of plaque mass on the packing pressure

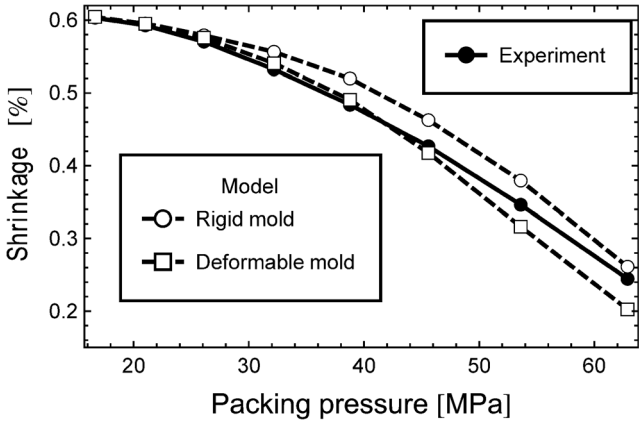

Fig. 13 Shrinkage dependence on packing pressure

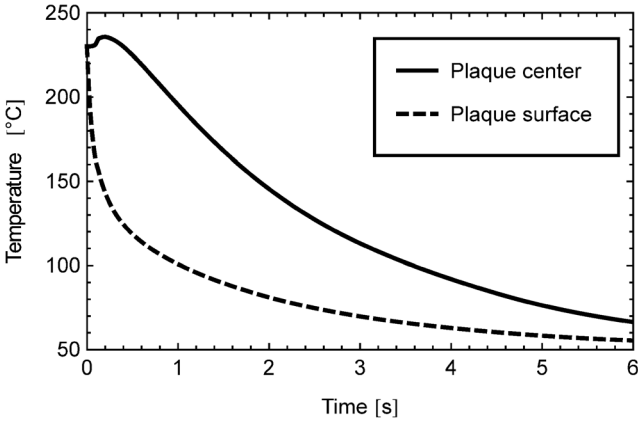

Fig. 15 Temperature evolution in the plaque center and at its surface

because higher pressures appear closer to the gate. The final mass factor also tended to be higher near the surface, which solidifies earlier, when the cavity pressure is higher. In the case of the deformable mold, larger final mass factor values appeared, because a deformed (i.e., higher) cavity accepts more material. Minor non-smoothness occurred at position P3 (see Fig. 5) due to non-smoothness of the spatial pressure interpolation (see Fig. 8). The cross section in Fig. 16 demonstrates the through thickness and flow path variation of the mass factor, while the variation in the y-direction is small and therefore not displayed.

Higher tensile stress in the plaque core is also evident for the rigid mold case in Fig. 17, which on a scaled longitudinal cross section, depicts the residual stress σ_x, as determined at packing pressure setting 8 for both cases of the mold deformability. Both cases exhibit a characteristic tensile core, enclosed by compressive layers. These results cannot be directly compared to the measurements of Zoetelief et al. [20] or Kamal et al. [12], who also analyzed polystyrene plaques, because the experimental conditions do not match. There, the cavity height was 2 and 3 mm, respectively. Nevertheless, they measured $\sigma_x = -2.5$MPa in the compressive region and $\sigma_x = 1$MPa in the core region which agrees in the order of magnitude with the results of this work. The variation of σ_x in the y-direction is small.

The spatial variation of pressure is also reflected in the final geometry, displayed in Fig. 18 for the deformable mold case and packing pressure setting 6; the displacements are scaled by a factor of 50. The width of the part varies with x, which is visible from the transverse local shrinkage contour plot. The final thickness likewise depends on the pressure distribution, especially evident in the gate proximity (i.e., near the origin). The in-plane local shrinkages in x- and y-directions are nearly equal, which agrees with the experiments of Jansen [17], where shrinkage was measured locally in both of the in-plane directions along the flow path. The local shrinkage distribution is experimentally unavailable, but the predictions are reasonable and are considered to be validated by the agreement of the total shrinkage at multiple pressures (Fig. 13).

In Fig. 19, the thickness shrinkage is displayed for both cases of mold rigidity and all packing pressure settings approximately at the cavity center. A significantly wider range of values is obtained than for the in-plane shrinkages. For the highest two packing pressure settings, wall expansion was predicted in the deformable mold case. This is expected, according to literature, where even values between 0 and −10% were measured in similar conditions [27]. Jansen et al. [17] also noted that the reports in literature vary significantly,

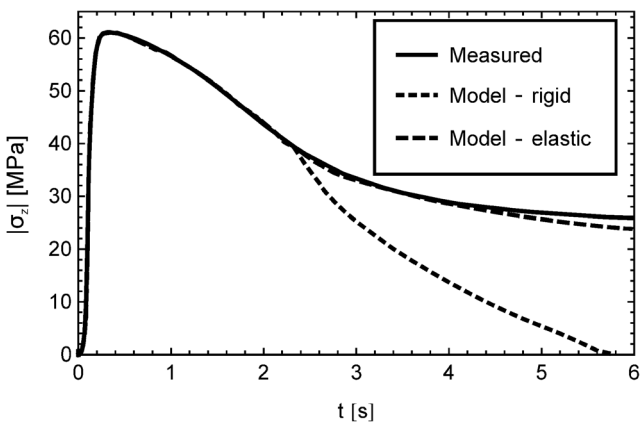

Fig. 14 Evolution of the absolute value of stress σ_z

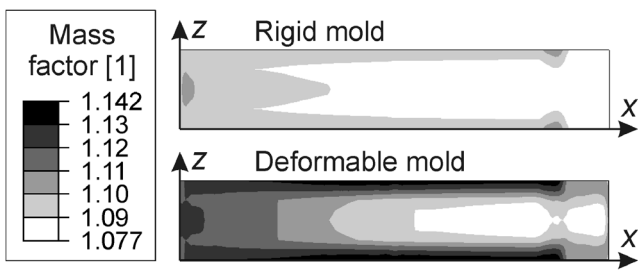

Fig. 16 Final mass factor distribution (a visually scaled longitudinal cross section)

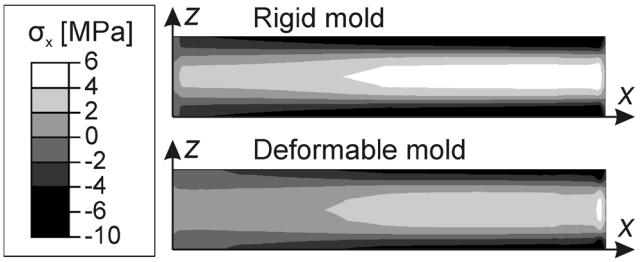

Fig. 17 Residual stress σ_x, determined with packing pressure setting 8 for rigid and deformable mold (a visually scaled longitudinal cross section)

which is reasonable, since the thickness shrinkage displays a strong dependence on the mold deformability. The effect of mold deformability is confirmed to be significant with our model, because a pronounced difference between the rigid and deformable mold cases was determined on increasing pressure. An experimental counterpart of Fig. 19 is not available, but our rudimentary thickness measurements showed a similar part thickness change in pressure.

6 Conclusion

An approach to stress evolution modeling in injection molding was presented. A simplification of the melt region was introduced by solving the equilibrium condition for this region as well, which is an alternative to excluding it from the model. Product mass was thus explicitly computed and also compared to the measurements in order to assess the validity of the approach.

The numerical implementation was elaborated only as far as necessary to test the modeling approach. This includes the assumption of elasticity of the solid region and the simplification of the geometry to a cuboid, thus leaving plenty of possibilities for improvement of the results themselves. As for the approach, it could, for example, be elaborated to model the melt region with an Eulerian mesh, which would allow predicting the fluid velocity field. But with growing complexity, the model could become difficult to manage in the scope of an applied study of a manufacturing process, especially at the point where custom code development becomes the only implementation possibility.

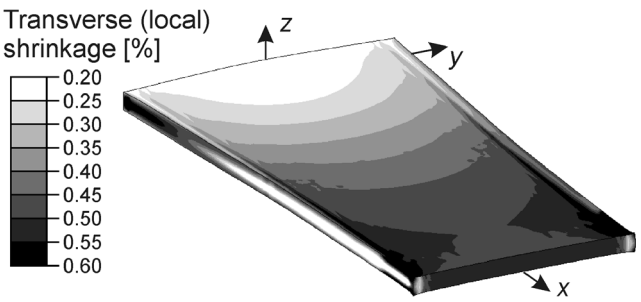

Fig. 18 Local transverse shrinkage displayed on the scaled final geometry—displacements scaled by factor 50

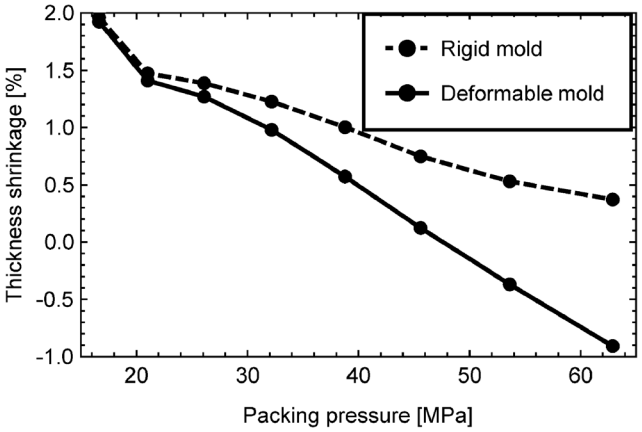

Fig. 19 Calculated thickness shrinkage at $x = 40$ mm and $y = 0$ mm

The predictive capabilities of the proposed approach are evident when a numerically obtained pressure field is imposed, and complex three-dimensional geometry is modeled in a general purpose simulation environment. This makes the approach appropriate for manufacturing oriented research. In the current work, the ejection stage modeling consisted only of finding the equilibrated thermo-mechanical state of the product, but the proposed approach could well be used to initiate a mechanical analysis of a non-trivial ejection, e.g., predicting the ejection force distribution over the ejector pins, ejector contact stress, and assessing the product integrity.

Acknowledgments This research did not receive any specific grant from funding agencies in the public, commercial, or not-for-profit sectors.

References

1. Kennedy P (2008) Practical and scientific aspects of injection molding simulation. Technische Universiteit Eindhoven, Endhoven, The Netherlands. http://www.worldcat.org/title/practical-and-scientific-aspects-of-injection-molding-simulation/oclc/723286754
2. Wang H, Kabanemi KK, Salloum G (2000) Numerical and experimental studies on the ejection of injection-molded plastic products. Polym Eng Sci 40:826–840
3. Kabanemi KK, Vaillancourt H, Wang H, Salloum G (1998) Residual stresses, shrinkage, and warpage of complex injection molded products: numerical simulation and experimental validation. Polym Eng Sci 38:21–37. doi:10.1002/pen.10162
4. Pontes AJ, Pouzada AS, Pantani R, Titomanlio G (2005) Ejection force of tubular injection moldings. Part II: a prediction model. Polym Eng Sci 45:325–332. doi:10.1002/pen.20275
5. Jansen KMB, Titomanlio G (1996) Effect of pressure history on shrinkage and residual stresses—injection molding with constrained shrinkage. Polym Eng Sci 36:2029–2040

6. Bataineh OM, Klamecki BE (2005) Prediction of local part-mold and ejection force in injection molding. J Manuf Sci Eng-Trans Asme 127:598–604
7. Marson S, Attia UM, Lucchetta G et al (2011) Flatness optimization of micro-injection moulded parts: the case of a PMMA microfluidic component. J Micromechanics Microengineering 21:115024
8. Titomanlio G, Jansen KMB (1996) In-mold shrinkage and stress prediction in injection molding. Polym Eng Sci 36:2041–2049
9. Bushko WC, Stokes VK (1996) Solidification of thermoviscoelastic melts. Part 4: effects of boundary conditions on shrinkage and residual stresses. Polym Eng Sci 36:658–675. doi:10.1002/pen.10454
10. Baaijens FPT (1991) Calculation of residual stresses in injection molded products. Rheol Acta 30:284–299. doi:10.1007/BF00366642
11. Chang R-Y, Chiou S-Y (1995) A unified K-BKZ model for residual stress analysis of injection molded three-dimensional thin shapes. Polym Eng Sci 35:1733–1747
12. Kamal MR, Lai-Fook RA, Hernandez-Aguilar JR (2002) Residual thermal stresses in injection moldings of thermoplastics: a theoretical and experimental study. Polym Eng Sci 42:1098–1114
13. Kang SY, Kim SK, Lee WI (2008) Penalty formulation for postfilling analysis during injection molding. Int J Numer Methods Fluids 57:139–155. doi:10.1002/fld.1630
14. Li X, Ouyang J, Li Q, Ren J (2012) Simulations of a full three-dimensional packing process and flow-induced stresses in injection molding. J Appl Polym Sci 126:1532–1545. doi:10.1002/app.36648
15. Spina R, Spekowius M, Dahlmann R, Hopmann C (2014) Analysis of polymer crystallization and residual stresses in injection molded parts. Int J Precis Eng Manuf 15:89–96. doi:10.1007/s12541-013-0309-2
16. Zheng R, Tanner RI, Fan X-J (2011) Injection molding. Springer Berlin Heidelberg, Berlin, Heidelberg
17. Jansen KMB, Van Dijk DJ, Husselman MH (1998) Effect of processing conditions on shrinkage in injection molding. Polym Eng Sci 38:838–846
18. Jansen KMB, van Dijk DJ, Burgers EV (1998) Experimental validation of shrinkage predictions for injection molded products. Int Polym Process 13:99–104. doi:10.3139/217.980099
19. Vietri U, Sorrentino A, Speranza V, Pantani R (2011) Improving the predictions of injection molding simulation software. Polym Eng Sci 51:2542–2551. doi:10.1002/pen.22035
20. Zoetelief WF, Douven LFA, Housz AJI (1996) Residual thermal stresses in injection molded products. Polym Eng Sci 36:1886–1896. doi:10.1002/pen.10585
21. Aho J, Syrjälä S (2008) On the measurement and modeling of viscosity of polymers at low temperatures. Polym Test 27:35–40. doi:10.1016/j.polymertesting.2007.08.004
22. Pantani R, Speranza V, Titomanlio G (2001) Relevance of mold-induced thermal boundary conditions and cavity deformation in the simulation of injection molding. Polym Eng Sci 41:2022–2035
23. Pouzada AS, Ferreira EC, Pontes AJ (2006) Friction properties of moulding thermoplastics. Polym Test 25:1017–1023. doi:10.1016/j.polymertesting.2006.06.009
24. Dawson A, Rides M, Nottay J (2006) The effect of pressure on the thermal conductivity of polymer melts. Polym Test 25:268–275. doi:10.1016/j.polymertesting.2005.10.001
25. CJ Y, Sunderland JE, Poli C (1990) Thermal contact resistance in injection molding. Polym Eng Sci 30:1599–1606. doi:10.1002/pen.760302408
26. Delaunay D, Le Bot P, Fulchiron R et al (2000) Nature of contact between polymer and mold in injection molding. Part I: influence of a non-perfect thermal contact. Polym Eng Sci 40:1682–1691. doi:10.1002/pen.11300
27. Jansen KMB, Pantani R, Titomanlio G (1998) As-molded shrinkage measurements on polystyrene injection molded products. Polym Eng Sci 38:254–264. doi:10.1002/pen.10186